Study on underwater two-dimensional exhaust vent mode based on fixed orifice spacing and variable orifice area distribution

Jun Suo*, *Hongbin* Wang, *Fei* Xu, and *Simi* Tang

Naval Research Institute, 100161 Beijing, China

Abstract. The scale parameters of bubbles produced by underwater exhaust influence the effect of the acoustic insulation. According to the dynamic characteristics in the process of underwater exhaust and the design criteria of equal flow per unit area, the two-dimensional equation of underwater exhaust was established. The analytical expressions of the orifice position and geometric parameters of the two-dimensional underwater exhaust device were obtained. The finite element models were established to compare the two vent patterns of uniform distribution and fixed orifice spacing / variable orifice area distribution. The exhaust effect was verified by circulating flume test. The simulation and experimental results show that the fixed orifice spacing and variable orifice area distribution mode can effectively control the distribution of bubbles scale parameters, and enhance the acoustic insulation effect of bubbles.

1 Introduction

With the continuous expansion of human development of marine activities, the noise pollution generated by industrial equipment in the process of transforming the ocean has attracted more and more attention. Increasing the noise control of underwater equipment is of great significance to the healthy development of the marine environment and ecosystem [1].

In terms of noise control of underwater equipment, the bubble curtain generating device can form an air curtain containing a large number of bubbles of different sizes in seawater, which has a strong attenuation and shielding effect on underwater noise [2], and is widely used in water system dredging [3], underwater drilling and blasting [4], acoustic control of fish repellent isolation [5] and other fields.

The bubble shape in the curtain has a significant influence on the acoustic control effect [6]. When a bubble is stimulated to resonate, its scattering cross section is more than 1000 times its geometric cross section. For a multi-body strong scatterer such as a bubble group, when the gas-liquid volume concentration is greater than 10^{-7}, the multiple scattering between bubbles cannot be ignored [7]. For decades, many scholars have conducted a lot of in-depth analysis and research on this problem, and have given the conclusion that the multi-body multiple scattering leads to a large increase of the damping coefficient of the

* Corresponding author: mrsuo@163.com

© The Authors, published by EDP Sciences. This is an open access article distributed under the terms of the Creative Commons Attribution License 4.0 (http://creativecommons.org/licenses/by/4.0/).

bubble group [8]. The experimental results of the bubble acoustic damping in the bubble curtain also show that the acoustic damping of a single ideal bubble is much smaller than the average acoustic damping of each bubble in the curtain. The multi-body multiple scattering of the bubble group is the main reason for increasing the sound attenuation of the bubble group [9].

In practice, the size and distribution of bubbles in the curtain have a significant impact on the acoustic damping and attenuation characteristics [10]. In order to obtain the rules of the preset bubble size and distribution, it is necessary to optimize the design of the bubble curtain generating device. Based on the analysis of the influence of the bubble curtain size distribution on the acoustic attenuation, this paper carries out a theoretical analysis of the orifice distribution of the bubble curtain generating device, and compares the quantitative effect of the uniform distribution and the fixed orifice spacing / variable orifice area distribution schemes by simulation and experiments.

2 Sound attenuation model of bubble curtain and its influence on sound propagation

2.1 Analysis of bubble scale distribution characteristics

The bubble distribution generated by the bubble curtain generating device can be divided into two types: symmetrical distribution (normal) and asymmetrical distribution. Numerous experimental measurements of bubbles by N. Davids & E. G. Thurston[11], F. E. Fox, et al.[12] and D. T. Laird & P. M. Kendig[13] have shown that the bubble population distribution function in water tends to asymmetrically distributed, and basically conforms to the Poisson distribution.

In the case of Poisson distribution, the distribution function $n(R)$ of bubbles can be written as:

$$n(R) = N_0 R^E e^{-\frac{ER}{R_0}}, \tag{1}$$

$$N_0 = \frac{\tau_N}{\int_0^\infty \frac{4}{3}\pi R^{3+E} e^{-\frac{ER}{R_0}} dR} \tag{2}$$

where R_0, E are two distribution constants. R_0 is the expected radius of the bubble under the Poisson distribution condition, E is the dispersion degree of the expected radius of the bubble, and τ_N is the volume concentration of the bubble group.

2.2 Analysis of acoustic performance of bubble curtain

Applying the bubble vibration equation, the reflection coefficient of the bubble curtain can be deduced as

$$IR = \frac{\left(1-k_1^2\right)\left(e^{-jk*d} - e^{jk*d}\right)}{(1-k_1)^2 e^{-jk*d} - (1+k_1)^2 e^{jk*d}}, \tag{3}$$

The transmission coefficient is

$$ID = \frac{1}{2}\left\{\left[k_1(1-IR)+(1+IR)\right]e^{-jk*d} - \left[k_1(1-IR)-(1+IR)\right]e^{jk*d}\right\}e^{jk_0 d}, \tag{4}$$

In (4), $k_1 = k_0 / k^*$, where k_0 is the wave number in a uniform liquid (water) without bubbles, and $k*$ is the equivalent complex wave number of the two-phase medium. $k* = \frac{\omega}{C*}$, where the bubble vibration frequency $\omega = \frac{1}{R}\sqrt{\frac{3\gamma p_0}{\rho}}$ (γ is the specific heat ratio of the gas, p_0 is the static pressure in the bubble, ρ is the liquid density). $C* = \sqrt{\frac{1}{\rho * \beta *}}$ ($\rho *$ is the gas-liquid mixing density, the equivalent complex compressibility $\beta* = \beta_0 - \int_0^\infty n(R)\frac{\partial v}{\partial p}dR$, $\frac{\partial v}{\partial p}$ is the compressibility of the bubble with radius R, β_0 is the compressibility of the desired radius of the bubble.

It can be seen from Equations (1), (2), (3) and (4) that the reflection coefficient IR and transmission coefficient ID of the bubble curtain are related to the bubble radius R, distribution characteristic E, volume concentration τ_N and thickness d of the bubble curtain.

The effect of the bubble radius R change on the transmittance (insertion loss) by τ_N, E and d fixed, are shown in the figure below.

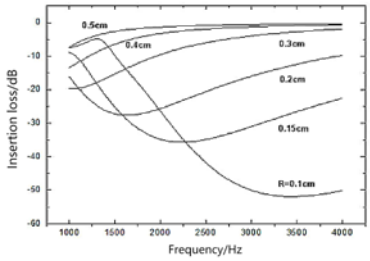

Fig. 1. Effect of bubble radius change on insertion loss.

The effect of bubble radius dispersion degree E on transmittance (insertion loss) by τ_N, R_0 and d fixed, are shown in the figure below.

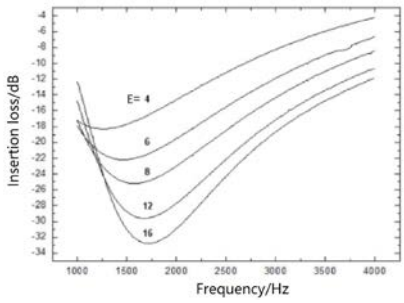

Fig. 2. Effect of bubble size distribution characteristics on insertion loss.

It can be seen that the sound insulation effect of the bubble curtain can be improved by adjusting the bubble size parameters in the bubble curtain. In view of this rule, this paper develops the parameter design of the bubble curtain generating device, and takes fixed

orifice spacing and variable orifice area as the design principle to achieve the bubble size as uniform as possible .

3 Design of fixed orifice spacing and variable orifice area of bubble curtain generating device

3.1 Basic assumption

In order to make the exhaust effect of the bubble curtain generating device uniform, the basic assumption of the design is that the exhaust air volume is equal per unit area. Based on this principle, the design of the fixed orifice spacing and variable orifice area of the exhaust orifices of the bubble generating device can be realized.

3.2 Theoretical derivation

Under the principle of equal volume exhaust per unit area, the orifice spacing is equal, and the area of each orifice is unequal to ensure that the flow rate of each orifice is equal.

According to the basic assumption, the flow rate of each orifice

$$Q = \frac{Q_0}{mn}, \tag{5}$$

where Q_0 is the total flow of the inlet, m, n are the numbers of rows and columns of the orifices. The jet velocity of the orifices in row i and column j

$$v_{ij} = \mu\sqrt{\frac{2}{\rho_{Hi}}\left(P_{ij} - P_{Hi}\right)}, \tag{6}$$

where μ is the orifice flow coefficient, ρ_{Hi} is the density of the gas of the orifices at the i-th row when the gas velocity v_{ij} is obtained, P_{ij} is the gas pressure of the orifice at the i-th row and j-th column, and P_{Hi} is the seawater static pressure of the orifices at the i-th row.

Combine the ideal gas equation

$$\rho_{Hi} = WP_{Hi}, \tag{7}$$

$$P_{ij} = \left(1 + \frac{D}{a_{ij}^2}\right)P_{Hi}, \tag{8}$$

where $D = \frac{WQ_0^2}{2m^2n^2\mu^2}$.

From the Bernoulli equation for incompressible fluid, we have

$$P_{i+1,j} + \frac{\rho_{i+1,j}V_{i+1,j}^2}{2} = P_{ij} + \frac{\rho_{ij}V_{ij}^2}{2} + \Delta P_{ij}, \tag{9}$$

where ΔP_{ij} is the resistance pressure along the path between the two cross-sections of the orifices from the i-th row to the row No. (i+1) on the j-th column, and V_{ij}, $V_{i+1,j}$ are the gas

flow rates in the vent pipe at the i-th row and the row No. (i+1) on the j-th column. From the assumption of uniform exhaust, we have

$$V_{ij} = \frac{Q_{ij}}{A_i} = \frac{Q_0 ij}{mnA_i},$$

$$V_{i+1,j} = \frac{Q_{i+1,j}}{A_{i+1}} = \frac{Q_0 (i+1) j}{mnA_{i+1}}, \tag{10}$$

where A_i is the equivalent cross sectional area of the vertical macroscopic gas flow of the orifices at the i-th row in the vent pipe.

The resistance pressure along the path

$$\Delta P_{ij} = \int_0^{\frac{h}{n-1}} \frac{\lambda}{d_i} \cdot \frac{\rho_{ij} V_{ij}^2}{2} dx = \frac{\lambda W P_{ij} Q_0^2 i^2 j^2 h}{2m^2 n^2 (n-1) d_i A_i^2} = \frac{\lambda h}{(n-1) d_i A_i^2} D\mu^2 i^2 j^2 P_{ij}, \tag{11}$$

where h is the overall height of the vent, λ is the resistance coefficient along the path, and d_i is the equivalent diameter of the cross section of the vent pipe at the current position.

Substituting Equations (8), (10), and (11) into Equation (9), we can get

$$a_{i+1,j} = \sqrt{\frac{D}{\frac{P_{Hi}}{P_{H,i+1}} \cdot \frac{1+\left[1+\frac{\lambda h}{(n-1)d_i}\right] i^2 j^2 \frac{D\mu^2}{A_i^2}}{1+(i+1)^2 j^2 \frac{D\mu^2}{A_{i+1}^2}} \left(1+\frac{D}{a_{ij}^2}\right) - 1}}. \tag{12}$$

Given the orifice area a_{1j} of a certain column in the first row farthest from the air intake of the vent pipe, the area a_{ij} of each orifice in this column can be obtained.

It can be obtained by the same mathematical operation

$$a_{i,j+1} = \sqrt{\frac{D}{\frac{1+\left[1+\frac{\lambda w}{(m-1)d_j}\right] i^2 j^2 \frac{D\mu^2}{A_j^2}}{1+i^2 (j+1)^2 \frac{D\mu^2}{A_{j+1}^2}} \left(1+\frac{D}{a_{ij}^2}\right) - 1}}. \tag{13}$$

Given the orifice area a_{i1} of a certain row in the first column farthest from the air intake of the vent pipe, the area a_{ij} of each orifice in this row can be calculated.

4 Finite element calculation and analysis of phase distribution and vent pressure in exhaust process

4.1 Basic idea

According to the principle of similar area and inlet pressure, the bubble curtain generating device models with uniformly distributed and fixed-spacing/variable-area exhaust orifices were established respectively. It was verified whether the uniform dispersion, the increased gas-liquid mixing area and the optimized distribution characteristics of bubble groups can be achieved.

4.2 Uniformly distributed vents model

A finite element meshed model of an exhaust device with open orifices (radius of 15mm) was established, as shown in Figure 3.

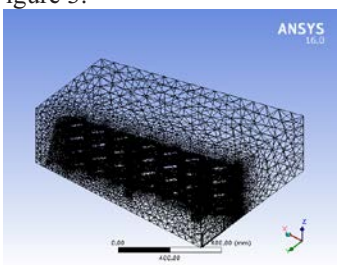

Fig. 3. Grid model of exhaust orifice scheme of uniform distribution of 2kg/s intake flow.

The number of the nodes is 139773. The number of the units is 751761. Using the Mixture model of two-phase fluid flow, the k- ε viscosity model, and the intake flow rate of 2kg/s, the gas injection situations are shown in Figure 4.

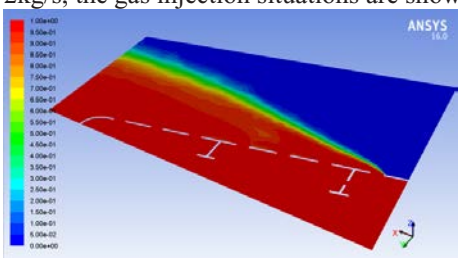

(a) z=526mm

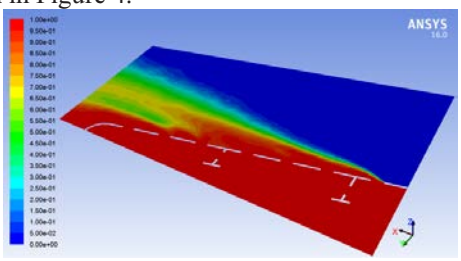

(b) z=376mm

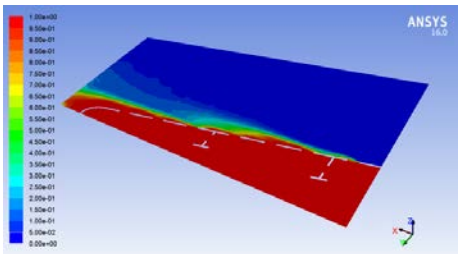

(c) z=226mm

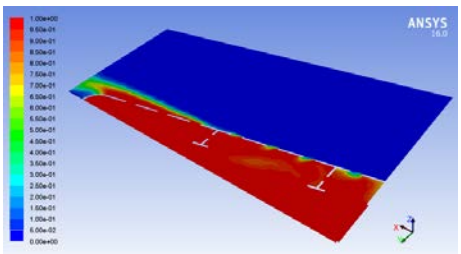

(d) z=76mm

Fig. 4. Longitudinal gas phase distribution of the uniformly distributed vent model (z is the distance from the bottom of the device, 2kg/s flow rate).

In the 2kg/s flow velocity uniform distribution vent model, the injection state of the lower orifices is very uneven compared with the upper orifices. It is unfavorable for the uniform distribution of bubbles that even backflow occurs in the lower orifices.

The pressure of the air inlet is 131575.45~132524.45Pa, and the pressure at the nearby exhaust orifice is 131575.45~132524.45Pa. The total area of the orifices is 112192.03mm^2.

The inlet pressure is related to the back pressure of the exhaust pipe. In the subsequent flow analysis of 2kg/s with fixed orifice spacing and variable orifice area design, maintaining the total area of the above-mentioned orifices or the pressure at the initial position of the intake air is the design basis, in order to ensure that the optimized design will not affect the back pressure of the exhaust pipe and other equipment parameters.

4.3 Vent model of fixed orifice spacing and variable orifice area

4.3.1 The principle of total orifice area approaching

The design principle is the total area of orifices closing to that of the uniformly distributed exhaust orifice model with a 2kg/s flow rate and a radius of 15mm. From Equations (12) and (13), the orifice area farthest from the air inlet is 1291.7mm^2, the margins of the upper and lower sides are 60mm, and the left and right 180mm. The total orifice area is 112282.26mm^2 with 7 columns and 4 rows. A finite element meshed model of the designed exhaust device was established, as shown in Figure 5.

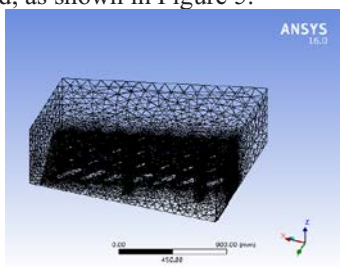

Fig. 5. Grid model of exhaust orifice scheme of fixed orifice spacing and variable orifice area of 2kg/s intake flow with the principle of total orifice area approaching.

The number of the nodes is 161693. The number of the units is 873200. Using the two-phase flow Mixture model, the k-ε viscosity model, the gas injection situations are shown in Figure 6.

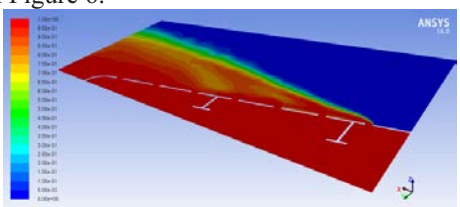

(a) z=548mm

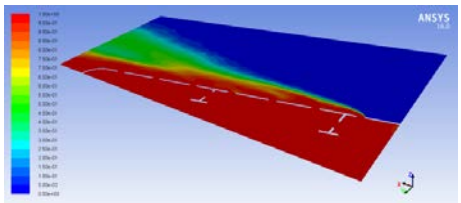

(b) z=402mm

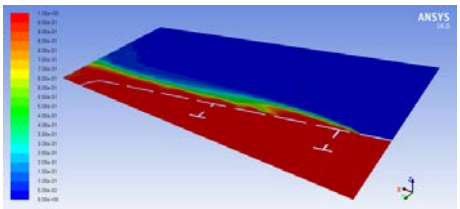

(c) z=257mm

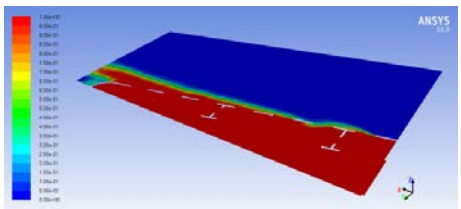

(d) z=122mm

Fig. 6. Longitudinal gas phase distribution of exhaust orifice model of fixed orifice spacing and variable orifice area with the principle of total orifice area approaching (z is the distance from the bottom of the device, 2kg/s flow rate).

It can be seen from the above figures that the model has relatively more uniform injections, especially in the lower layer to avoid the phenomenon of seawater backflow, compared with the uniformly distributed vent model.

The air inlet pressure is 133386.08~136103.86Pa, and the pressure at the nearby exhaust orifice is 133386.08~136103.86Pa. Compared with that of the uniformly distributed vent model, the pressure at the inlet and the nearby orifice is slightly 2.04% higher.

The above analysis shows that the pressures of the intake port and the nearby exhaust orifice are basically the same as the design pressure of the uniformly distributed exhaust vent within the deviation 2.57% under the condition that the total orifice area is approaching.

4.3.2 The principle of pressure approaching at the initial position of the intake air

The pressure of the orifice at the initial position of the intake air in the uniformly distributed exhaust model is 131575.45~132524.45Pa under the condition of flow rate 2kg/s, orifice radius 15mm, according to the finite element calculation. With this pressure as the design principle, a reasonable orifice design method can be obtained: the farthest orifice is 720mm^2, the margins of the upper and lower sides are 60mm, the left and right 180mm with 7 columns and 4 rows. The pressure of the nearby orifice is 132016.25Pa. The total area of the orifices is 22272.46 mm^2. A finite element meshed model of the designed exhaust device was established, as shown in Figure 7.

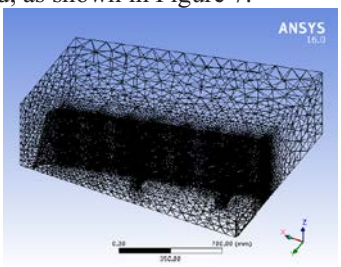

Fig. 7. Grid model of exhaust orifice scheme of fixed orifice spacing and variable orifice area of 2kg/s intake flow with the principle of pressure approaching at the initial position of the intake air.

The number of the nodes is 219955. The number of the units is 1193025. Using the two-phase flow Mixture model, the k- ε viscosity model, the gas injection situations are shown in Figure 8.

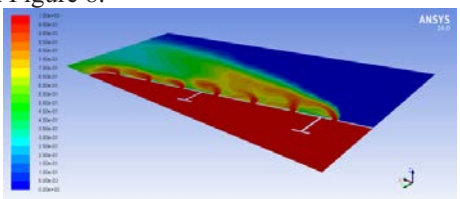

(a) z=546mm

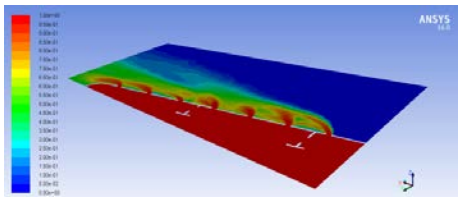

(b) z=400mm

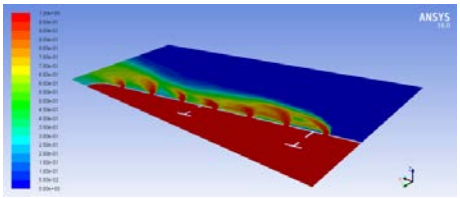

(c) z=253mm

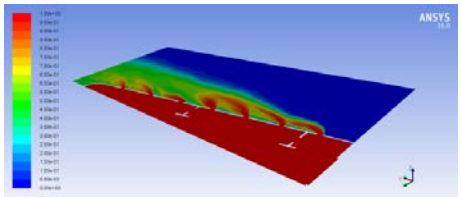

(d) z=107mm

Fig. 8. Longitudinal gas phase distribution of exhaust orifice model of fixed orifice spacing and variable orifice area with the principle of pressure approaching at the initial position of intake air (z is the distance from the bottom of the device, 2kg/s flow rate)

It can be seen from the above figures that the orifice area is smaller and a uniform gas injection structure can be formed under this design condition.

The air inlet pressure is 199968.27~211845.58Pa, and the pressure at the nearby exhaust orifice is 140581.67~152459.00Pa. Compared with the nearby orifice pressure 132016.25Pa by analytical calculation, the difference between the two methods is about 9.90%.

5 Exhaust test verification

According to the parameters in Section 4, the verification models are shown in Figure 9. and 10.

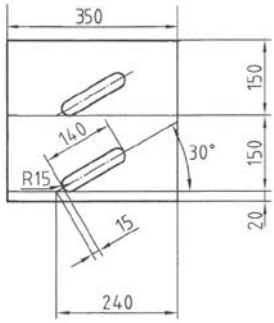

Fig. 9. Uniformly distributed exhaust model.

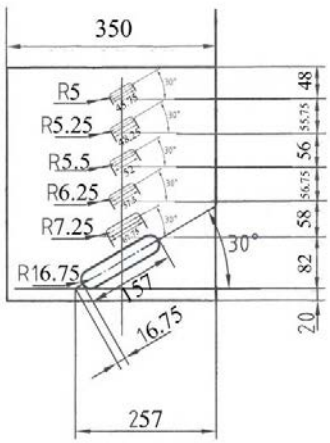

Fig. 10. Fixed orifice spacing and variable orifice area exhaust model.

The exhausted bubble states of different models were observed in the circulating flume, as shown in Figures 11 and 12. The test main parameters are shown in Table 1.

Fig. 11. Exhaust situation of uniformly distributed exhaust model.

Fig. 12. Exhaust situation of fixed orifice spacing and variable orifice area exhaust model.

Table 1. Test main parameters.

Flume depth/m	Bottom orifice depth/m	Water flow rate/$m^3 \cdot h^{-1}$
1.6	1.45	300

1000 bubbles were investigated in each situation under the same exhaust condition. The average diameter of the bubbles is about 7.95mm, the median diameter is about 5.47mm, and the variance is about 0.75mm^2 in the uniform exhaust mode, nearly without exhaust in the bottom vent orifices. The average diameter of the bubbles is about 3.24mm, the median diameter is about 2.75mm, and the variance is about 0.33mm^2 in the fixed orifice spacing and variable orifice area exhaust mode. The bottom vent orifices can maintain uniform exhaust like the upper. The exhaust effect of the fixed orifice spacing and variable orifice area model is obviously better than that of the uniform exhaust model.

6 Conclusions

In this paper, the theoretical analysis of the orifice design of the bubble curtain generating device is carried out, and the quantitative effects of different schemes are compared by simulation and experimental verification.

(1) The distribution function of bubble groups in water basically conforms to the Poisson distribution. By adjusting the bubble size parameters in the bubble curtain, the sound insulation effect of the bubble curtain can be improved.

(2) The design of fixed orifice spacing and variable orifice area is carried out according to the principle of the equal exhaust air volume per unit. Under the principle of total orifice area approaching, the pressures of the intake port and the nearby exhaust orifice are basically the same as the designed pressure of the uniformly distributed exhaust vent. The deviation is within 2.57%. Compared with the analytical calculation, the pressure difference is about 9.90%.

(3) Under the same exhaust conditions, the exhaust effect of the fixed orifice spacing and variable orifice area exhaust model is obviously better than that of the uniform exhaust model.

References

1. G. S. Zhang, X. X. Gu, B. B. Xing, J. Dalian Ocean Univ., **27**(1), 89-94 (2012)
2. M. Minnaert, Phil.Mag., **26**, 235 (1933)
3. H. Y. Wang, F. X. Zhang, C. Liu, Water Resour. Power, **37**, 228(08), 12-15 (2019)
4. X. L. Lu, X. Q. Liang, G. C. Hu , et al., Blasting, **2**, 23-28 (2006)
5. J. Luo, Y. Q. Bai , C. Y. Lin, et al., Acta Hydrobiol. Sinica, **39**(5), 1065-1068 (2015)
6. W. G. Zhang, H. B. Wang, The 4th Ship Water Noise Symp., 24-27 (1991)
7. Z. W. Qian, Acta Phys. Sinica, **30**: 442-447 (1981)

8. A. I. Eller, J. Acoust. Soc. Am., **47**, 1469-1470 (1970)
9. Z. Qian, J. Sound &Vib., **168**, 327 (1993)
10. P. C. Waterman, J. Acoust. Soc. Am., **45**, 1417-1429 (1969)
11. N. Davids, E. G. Thurston, J. Acoust. Soc. Am., **22**, 20-33 (1950)
12. F. E. Fox, S. R. Curley, G. S. Larson, J. Acoust. Soc. Am., **27**, 534-539 (1955)
13. D. T. Laird, P. M. Kendig, J. Acoust. Soc. Am., **24**, 29-32 (1952)